UC Berkeley
UC Berkeley Previously Published Works

Title
High-resolution photoelectron spectroscopy of vibrationally excited TiO2 anions

Permalink
https://escholarship.org/uc/item/9dx832k4

Journal
The Journal of Chemical Physics, 165(17)

ISSN
0021-9606

Authors
Vlahos, Korina
Bole, Jacob
Zheng, Qing-Yi
et al.

Publication Date
2026-11-07

DOI
10.1063/5.0355313

Copyright Information
This work is made available under the terms of a Creative Commons Attribution-NonCommercial-NoDerivatives License, available at https://creativecommons.org/licenses/by-nc-nd/4.0/

Peer reviewed

eScholarship.org Powered by the California Digital Library
University of California

6 August 2026

High-Resolution Photoelectron Spectroscopy of Vibrationally Excited TiO2 Anions

Korina Vlahos[1], Jacob Bole[1], Qing-Yi Zheng[1], Walt Yang[1], Melinda Nolten[2], Martina Havenith[2], Daniel M. Neumark[1]

1. Department of Chemistry, University of California

2. Faculty of Chemistry and Biochemistry, Ruhr-Universität Bochum

Abstract

High resolution photoelectron spectra of TiO_2^- excited to its $\#_3$ = 1 state were obtained via slow electron velocity-map imaging of cryogenically cooled anions (cryo-SEVI). To determine the $\#_3$ (antisymmetric stretch) anion frequency, growth and depletion of various features in the cryo-SEVI spectrum were monitored over a range of infrared (IR) excitation energies. Photoelectron scans were taken at an IR pre-excitation energy of 918 cm^{-1} and yielded a ~6% depletion of features in the ground state cryo-SEVI spectra as well as new hot and sequence bands based on the 3_1^0 and 3_1^1 transitions, respectively. By monitoring hot band intensities as a function of IR laser frequency, the rotational profile of the $\#_3 = 0 - 1$ transition was mapped out and found to be centered at 914(7) cm^{-1}. The observed hot bands are Franck-Condon forbidden and arise from Herzberg-Teller coupling with the $\tilde{A}^1B_2$ neutral excited state, similar to what was observed in the cryo-SEVI spectra of TiO_2^-. The results from this IR cryo-SEVI experiment lay the groundwork for future investigations of larger bare and complexed transition metal oxide clusters.

Keywords

titania, photoelectron spectroscopy, cryogenically cooled clusters, IR excitation

Posted on 6 August 2026 — CC-BY-NC-ND 4.0 — This is a preprint and has not been peer reviewed. Data may be preliminary. — https://doi.org/10.26434/chemrxiv.15007122/v1

High-Resolution Photoelectron Spectroscopy of Vibrationally Excited TiO_2 Anions

Korina Vlahos [a], Jacob Bole [a], Qing-Yi Zheng [a] , Walt Yang [a] , Melinda Nolten [b], Martina Havenith [b] and Daniel M. Neumark [a]*

[a]Department of Chemistry, University of California, Berkeley, CA 94720, USA

[b]Ruhr-Universität Bochum, Faculty of Chemistry and Biochemistry Universitätsstraße 150 Building NC 7/72, D-44780 Bochum, Germany

Key words: titania, photoelectron spectroscopy, cryogenically cooled clusters, IR excitation

Abstract:

High resolution photoelectron spectra of TiO_2^- excited to its $v_3 = 1$ state were obtained via slow electron velocity-map imaging of cryogenically cooled anions (cryo-SEVI). To determine the ν_3 (antisymmetric stretch) anion frequency, growth and depletion of various features in the cryo-SEVI spectrum were monitored over a range of infrared (IR) excitation energies. Photoelectron scans were taken at an IR pre-excitation energy of 918 cm^{-1} and yielded a ~6% depletion of features in the ground state cryo-SEVI spectra as well as new hot and sequence bands based on the 3_1^0 and 3_1^1 transitions, respectively. By monitoring hot band intensities as a function of IR laser frequency, the rotational profile of the $v_3 = 0 - 1$ transition was mapped out and found to be centered at 914(7) cm^{-1}. The observed hot bands are Franck-Condon forbidden and arise from Herzberg-Teller coupling with the $\widetilde{A}^1B_2$ neutral excited state, similar to what was observed in the cryo-SEVI spectra of TiO_2^-. The results from this IR cryo-SEVI experiment lay the groundwork for future investigations of larger bare and complexed transition metal oxide clusters.

I. Introduction:

Transition metal oxides (TMOs) play a major role in many areas of catalysis. Notable examples include the conversion of N_2 to NH_3 by the Haber-Bosch process,[1] the catalytic oxidative dehydrogenation of hydrocarbons by vanadia,[2] and photoinduced water splitting on titania.[3] Although aspects of this chemistry has been known for many years, elucidation of the underlying mechanisms remains a very active area in experimental and theoretical physical chemistry.[4, 5] The importance of metal oxide catalysis has stimulated interest in the reactivity and spectroscopy of transition metal oxide clusters in gas phase, which can be thought of as finite-sized model systems for catalysts.[6]

In the gas phase, the size-dependent evolution of the structure and energetics of TMO clusters has been obtained primarily by two methods: infrared photodissociation spectroscopy (IRPD)[7-9] and anion photoelectron spectroscopy (PES).[10, 11] IRPD yields vibrational frequencies of size-selected cation and anionic clusters, while anion PES yields the electron affinity of the neutral cluster or,

in less favorable cases, the vertical detachment energy of the anion. Anion PES can also map out the electronic structure of the neutral cluster, and, depending on the system and the experiment, yield vibrationally resolved features in one or more neutral electronic states.

As one of the most powerful and versatile experimental methods in the chemical physics toolbox, anion PES has been applied to many other species of interest to physical chemistry, such as reactive free radicals[12] and transition states.[13] However, conventional PES experiments have somewhat limited energy resolution, typically around 100-300 cm^{-1}, so one is often unable to resolve vibrational structure in the PE spectrum of complex molecules and clusters. We have addressed this issue in our laboratory through slow-electron velocity-map imaging of cryogenically cooled anions (cryo-SEVI), a high resolution variant of PES that utilizes a tunable dye laser to detach electrons and a velocity-map imaging (VMI) spectrometer to measure their kinetic energies (eKEs), allowing for low-eKE measurements with sub-meV resolution.[14-16] This method has been used in our laboratory and elsewhere[17, 18] to obtain PE spectra of atoms, molecules, and clusters with energy resolution as high as 1-2 cm^{-1}. As relevant examples, we have carried out cryo-SEVI experiments several bare[19-22] and complexed[23-26] transition metal oxide clusters, obtaining spectra with extensive and well-resolved spectra for species such as $TiO_3H_2^-$, a di-hydroxide anion that results from the splitting of H_2O by TiO_2^-.[23] Here, we report the cryo-SEVI spectrum of TiO_2^- that is vibrationally pre-excited to its $v_3 = 1$ level prior to photodetachment.

The work presented here is an example of the recent incorporation of a tunable infrared (IR) laser into the cryo-SEVI instrument to vibrationally pre-excite negative ions prior to photodetachment. This new experiment, referred to as IR cryo-SEVI,[27] brings two additional capabilities. First, photodetachment from vibrationally excited anions enables one to access neutral vibrational levels that cannot be reached from the ground state. For example, the $v = 1$ levels of non-totally symmetric neutral vibrational modes have zero Franck-Condon overlap with the anion ground vibrational state but are easily reached from the corresponding v=1 anion levels. Secondly, IR cryo-SEVI can be run in an "action-spectroscopy" mode where one monitors depletion and growth of features in the PE spectrum as the IR laser is tuned, thereby mapping out vibrational transitions in the anion. We have previously reported studies on several molecular negative ions via IR cryo-SEVI.[28-31]

The application of IR cryo-SEVI to TiO_2^- presented herein represents a first step in using this method to investigate more complex TMO clusters. There are several challenges associated with these experiments. First, although TMOs have strong IR bands associated with metal-oxygen stretching vibrations, the frequencies of these vibrations tend to lie below 1000 cm^{-1}, where the power of our IR laser is quite low. Secondly, as shown in our study of the vinoxide anion ($C_2H_3O^-$),[29] effects from intramolecular vibrational redistribution (IVR) can complicate the IR cryo-SEVI spectra through anharmonic coupling in both the anion and neutral. Whether this happens in TMO clusters depends on the extent to which the IR active metal-oxide vibrations are coupled to other modes of the cluster. For TiO_2^-, a system for which we already have a high quality

cryo-SEVI spectrum,[19] one expects IVR to be minimal owing to its small size, making it a good test system for TMO IR cryo-SEVI.

Hence, we report IR cryo-SEVI spectra on TiO_2^- in which the ν_3 antisymmetric stretch mode of the anion is excited. Upon excitation of the ν_3 mode, we observe depletion of features from the ground state cryo-SEVI spectra and growth of new peaks corresponding to sequence and hot bands. By tracking the growth of new features over various IR excitation energies, we obtain an action spectrum that yields the experimental ν_3 frequency of 914 cm^{-1}. All new features in the IR cryo-SEVI spectra are assigned to hot and sequence bands originating from the TiO_2^- ($v_3 = 1$ level); some are reproduced in FC simulations, while others are FC-forbidden and are seen because of Herzberg-Teller coupling to a low-lying excited state of TiO_2.

II. Experimental Technique:

The IR-cryo-SEVI apparatus has been described in detail previously.[16, 27, 32] To form TiO_2^- anions by laser ablation, a 20 Hz Nd:YAG [Litron Nano S] laser (10-15 mJ/pulse) generates frequency-doubled light at 532 nm that is focused onto a pure titanium metal target to create a plasma, which is entrained in a pulse of He gas from an Even-Lavie valve[33] to quench the plasma and form the anion of interest. This arrangement is sufficient to form the target anion TiO_2^- due to residual oxides on the Ti target.

The newly formed ions are transported through a radiofrequency (RF) hexapole ion guide and quadrupole mass filter for pre-mass selection before entering a 5K cooled RF octupole ion trap. Here, the ions are collisionally cooled for ~40 ms by a pulsed buffer gas mixture of 80/20 He/H_2 at a pressure of around 10^{-3} Torr in the trap, resulting in internal temperatures of around 10 K. The ions are then extracted into an orthogonal Wiley-McLaren time-of-flight mass spectrometer,[34] where the mass-separated ions are focused into the interaction region of a velocity-map imaging (VMI) spectrometer.[35] In this region, the target anions are first vibrationally excited by a tunable OPO/OPA and then photodetached by a tunable dye laser. The IR OPO/OPA [LaserVision] is pumped by a 10 Hz Nd:YAG laser [Continuum SureLite SLIII-EX], where the far IR wavelengths (900-935cm^{-1}) are generated by difference frequency mixing of the OPA signal and idler output in a $AgGaSe_2$ crystal. With this setup, typical pulse energies of ~250μJ and pulse bandwidths of 3.5 cm^{-1} are obtained. The dye laser [Radiant Dyes NarrowScan] is pumped by the second harmonic of another 20 Hz Nd:YAG laser [Spectra-Physics Quanta-Ray PRO-290] to produce a photon detachment energy range of 1.30-2.20 eV (2-6 mJ/pulse), which was sufficient for this system. The counter-propagating IR and detachment beams are focused into the laser interaction region via a 500 mm ZnSe and 1000 mm CaF_2 lens, respectively, to ensure temporal and spatial overlap.

Photoelectrons detached in the interaction region of the VMI spectrometer are captured by a 2D position-sensitive detector that consists of two chevron-stacked multichannel plates coupled to a phosphor screen. After every laser shot, the electrons are photographed by a CCD camera[36] and

analyzed by an event-counting algorithm. These individual electron events are centroided and binned into a 1024 x 1024-pixel grid. This algorithm has additional ability to perform a centroid analysis of overlapping spots, which improves the efficiency of data collection.[37] The sum of these electron events result in VMI images that are processed with the maximum entropy Legendre expanded image reconstruction (MELEXIR) method[38] to obtain radial and angular distributions. The radial distribution is related to the electron kinetic energy (eKE) by calibrating with several well-known detachment energies of O^-.[39] All spectra are reported in electron binding energy (eBE), given by eBE = $h\nu$ – eKE.

Photoelectron angular distributions (PADs), are characterized by the anisotropy parameter β according to[40-42]

$$\frac{d\sigma}{d\Omega} = \frac{\sigma_{tot}}{4\pi}[1 + \beta P_2(\cos\theta)], \quad (1)$$

where σ_{tot} is the total detachment cross section, P_2(x) is the second-order Legendre polynomial, and θ is the angle of the outgoing photoelectron velocity vector with respect to the laser polarization axis. The anisotropy parameter ranges from -1 (perpendicular detachment) to +2 (parallel detachment) and provides information on the electronic character of each photodetachment transition.

The anion frequency of our mode of interest is first determined by monitoring the integrated peak area change between scans with (IR on) and without (IR off) pre-excitation over a range of IR energies, referred to as an IR action scan. Specifically, peak area growth is measured for new features starting at $v_3 = 1$ in the anion while depletion is measured for features from $v_3 = 0$ in the anion. After this scan, high resolution IR-cryo-SEVI spectra are taken at various photodetachment energies with the IR pre-excitation energy that produced the most depletion and growth , ensuring sub-meV resolution for relevant features. The IR-on and IR-off scans are taken concurrently to allow for direct shot-to-shot comparisons. From here, difference spectra are obtained by subtracting the IR-on scan from the IR-off scan to highlight the depletion and growth from pre-excitation.

III. Computational Methods:

Electronic structure calculations were carried out at the CCSD level and aug-cc-pVDZ basis set for both neutral and anionic TiO_2 on version 6.0 of the QChem software package.[43] The calculated equilibrium geometries and harmonic frequencies for both species are reported in Tables S1 and S2. The ν_2 bending mode is predicted to be at 308 cm^{-1}, which is outside the regime of accessible IR excitation energies. The ν_1 symmetric stretching mode is predicted at 970 cm^{-1} with an IR intensity of 210 km/mol in the anion, while the ν_3 antisymmetric stretching mode is predicted at 908 cm^{-1} with an IR intensity of 455 km/mol. Based on its larger calculated IR intensity, the ν_3 mode was considered the best candidate for an IR cryo-SEVI experiment.

Franck-Condon (FC) profiles for detachment from the anion ν_3=0 and 1 states were calculated using the calculated equilibrium geometries and normal modes using version 1.2 of the ezFCF software package.[44] The vibrational modes were treated within the harmonic approximation and using full Duschinsky to account for differences between the anion and neutral normal modes when calculating FC overlap integrals. For excited state detachment, the profile was simulated at 300K and FC factors for the features of interest were extracted. To model the action scan profiles, a PGOPHER simulation of the rovibrational profile for the ν_3 mode was done at a rotational temperature of 15K.

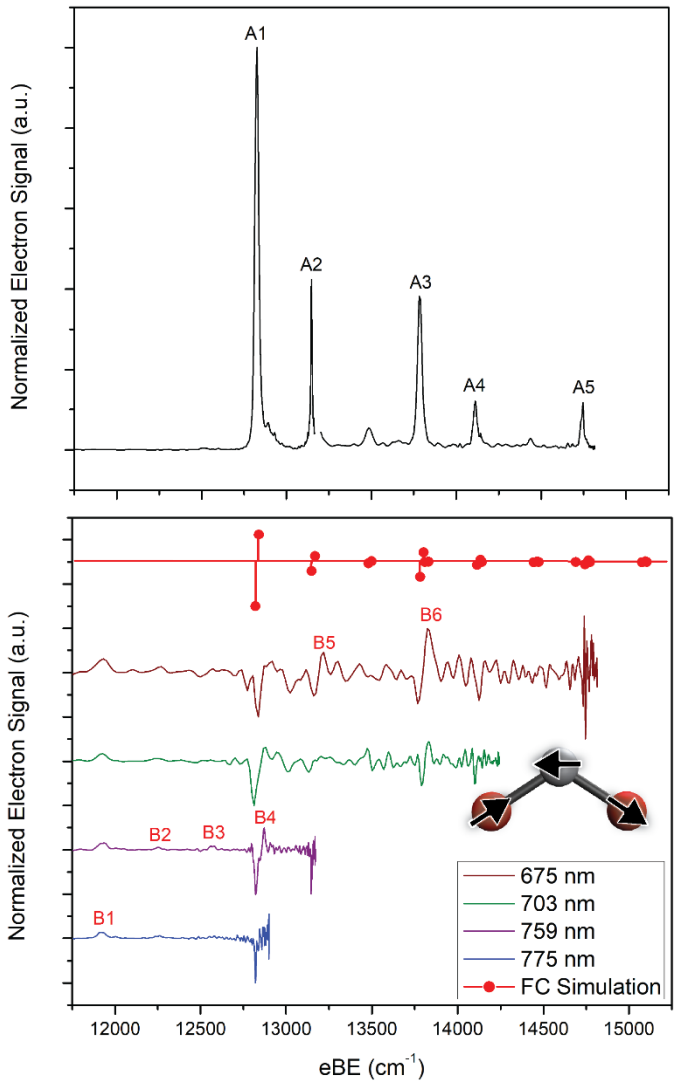


Figure 1: Top panel: Spliced high-resolution IR-off (black trace) cryo-SEVI spectra with transitions starting from $v = 0$ in the anion labeled. Bottom panel: Difference spectra (IR on-IR off) taken at a IR pre-excitation energy of 918 cm^{-1} and progressively lower photodetachment energies. A FC simulation (red trace) for photodetachment from the ν_3 fundamental mode, assuming a 6% origin depletion is also shown.

IV. **Results and Discussion**:

Anion ν_3 Fundamental Frequency Determination:

The high resolution cryo-SEVI spectrum for TiO_2^- shown in the top panel of Figure 1 has been previously reported and assigned.[19] Here, we explore the changes in this spectrum induced by excitation of the anion ν_3 mode. To determine the optimal IR excitation energy, a range of different frequencies, based on the electronic structure calculations, was explored to search for maximal depletion of the vibrational origin transition (peak A1) or growth of new features (peaks B1-3). This procedure led to the selection of 918 cm^{-1} as the optimal frequency to investigate the effects of IR excitation.

The bottom panel of Figure 1 shows the difference spectra (IR on – IR Off) taken at progressively lower detachment energies in order to better resolve the different features. Upon excitation at 918 cm^{-1}, there is a ~6% peak area depletion of features (A1-5) from the ground state cryo-SEVI spectra labeled in Figure 1. In addition to the depletion of ground state

features, three new peaks grow below the origin (B1-3) and three additional peaks (B4-B6) appear, each located around 20 cm^{-1} above a depletion feature. Peaks B4-B6 are in a noisier region of the difference spectrum since the IR-off signal is non-zero in their vicinity, whereas there is no IR-off intensity in the region where peaks B1-B3 occur. Peak positions, assignments, and shifts for each feature are also summarized in Table 1. The assignments of these new features will be discussed below based on the FC simulation (red trace) shown in Figure 1.

Using procedures described previously, [28, 31] we can then map out the rotational profile of the ν_3 mode in the "action spectroscopy" mode where either depletion of ground state features and/or growth of new features are followed as the IR laser is scanned. Figure 2 shows the action spectra when monitoring the total intensity of peaks B1-B3 over a scanning range of 900-930 cm^{-1} with 2 cm^{-1} steps and a detachment energy of 775 nm. The summed intensity of peaks B1-B3 was the most consistent and reliable feature to monitor since the IR-off signal has no intensity in this spectral region.

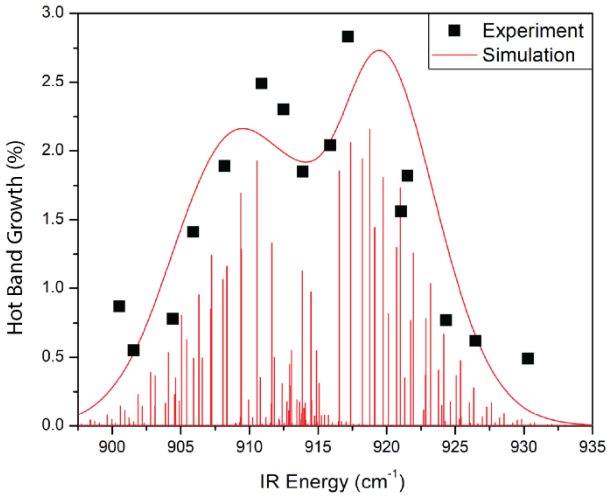


Figure 2: IR action spectra monitoring general hot band growth (black squares) is overlayed with a PGOPHER simulation (red sticks), assuming a vibrational band center of 915 cm^{-1} and an ion temperature of 15K. The simulation is also Gaussian broaden by 3 cm^{-1} (red curve).

From the action scan, a profile with a measured vibrational band center of 914 cm^{-1} is observed, placing the anion ν_3 antisymmetric Ti-O stretching mode at that frequency. The action spectrum is simulated using PGOPHER,[45] shown in Figure 2 (red trace). In these simulations, rotational constants derived from CCSD calculations ($A = 0.261\ cm^{-1}$, $B = 0.211\ cm^{-1}$, $C = 1.11\ cm^{-1}$) were used as well as a vibrational band center of 914 cm^{-1} and an ion temperature of 15K. With this good agreement, the ν_3 fundamental mode is placed at 914(7) cm^{-1}, close to the predicted anion frequency of 908 cm^{-1} from our CCSD calculations.

Table 1: Summary of the peak positions and their shifts from the 3_1^0 transition (B1) as well as the sign of the anisotropy parameter (β) and vibrational assignments for features in the IR-cryo-SEVI spectra of TiO_2^-.[a]

Peak	eBE (cm^{-1})	Assignment	Shift from 3_1^0	Anisotropy
B1	11 922 (24)	3_1^0	-	−
B2	12 257 (26)	$3_1^0 2_0^1$	335	−
B3	12 560 (16)	$3_1^0 2_0^2$	646	−
A1[b]	12 818	0_0^0	896	+
B4	12 870 (6)	3_1^1	948	+
A2[b]	13 147	2_0^1	1225	+
B5	13 216 (13)	$3_1^1 2_0^1$	1294	+
A3[b]	13 781	1_0^1	1859	+
B6	13 834 (21)	$3_1^1 1_0^1$	1912	+
A4[b]	14 109	$1_0^1 2_0^1$	2167	+
A5[b]	14 740	1_0^2	2818	+

[a]Uncertainties in the peak positions correspond to one standard deviation (σ) obtained from Gaussian fits of the highest resolution scan, which is related to the full width half maximum (FWHM) by $\mathrm{FMHM} = 2\sqrt{2\ln 2}\,\sigma$.

[b]Peak positions, assignments, and anisotropy are previously reported from Ref 55.

Vibrational Assignments:

Features B4-6 can be easily assigned based on the good agreement with the FC simulation shown in the bottom panel of Figure 1 (red trace). Neutral frequencies from our previous TiO_2^- study and the experimentally determined anion ν_3 frequency were used in the FC simulation. B4 lies slightly above the vibrational origin and is assigned to the 3_1^1 sequence band. The other peaks, B5 and B6, are assigned as 3_1^1 combination bands involving the ν_2 and ν_1 mode, respectively, as indicated in Table 1. Overall, the sequence bands terminate to vibrational states observed in the ground state cryo-SEVI spectra and appear with a slightly higher eBE shift due to the pre-excitation along the ν_3 mode. These transitions highlight the ability of this experiment to access neutral states that are FC forbidden from the anion ground state.

In contrast, transitions B1-3 do not appear in the FC simulation. Their PADs also differ from peaks B4-B6. Peaks B1-3 have a negative anisotropy parameter ($\beta<0$), while the other transitions have a positive anisotropy ($\beta>0$), as summarized in Table 1. Each transition appears ~900 cm^{-1} below the corresponding feature A1-3 and is thus assigned to a 3_1^0 hot band or combination band as seen in Table 1. Peaks B1-B3 are thus FC forbidden owing to the ν_3 mode being non-totally symmetric.

However, these transitions can appear in the spectra via Herzberg-Teller (HT) coupling by borrowing electronic character from a nearby coupled excited state.[23, 30] FC forbidden transitions involving the ν_3 mode were also present in the cryo-SEVI spectra of TiO_2^- and were attributed to HT coupling with the lowest lying excited singlet neutral state ($\widetilde{A}^1B_2$).[19] We assume that the same HT coupling mechanism is operative here.

Compared to previous IR-cryo-SEVI systems,[29-31] significantly less depletion and growth upon IR excitation is observed, despite the TiO_2^- ν_3 mode having a high calculated IR intensity. This is most likely due to the combination of very low power in the far IR and the broad linewidth (~30 cm^{-1}) of the action scan and calculated rotational profile. This broad profile means that a small fraction of ions lies within the bandwidth of the IR pulse, limiting the total amount of depletion and growth. In larger clusters such as $Zr_2O_4^-$, the rotational profile should be narrower owing to smaller rotational constants Outside these limitations, the experimental success of applying this technique to the ν_3 fundamental frequency of TiO_2^- shows considerable promise for future IR cryo-SEVI studies of other TMO clusters.

V. Conclusions:

High resolution photoelectron spectra of vibrationally pre-excited TiO_2^- ($v_3 = 1$) anions are reported. IR excitation at 918 cm^{-1} results in a ~6% depletion of features from the ground state cryo-SEVI spectra and the appearance of six new transitions. Through FC simulations, three new features (B4-6) lying slightly above ground state features were assigned as sequence and combination bands based on the 3_1^1 transition. Features lying below the vibrational origin were assigned to hot bands (3_1^0) and were absent in the simulation as they are FC-forbidden. The presence of these peaks is attributed to HT coupling with the $\widetilde{A}^1B_2$ excited neutral state. In addition to the photoelectron spectra, action scans monitoring the growth of hot bands over various IR pre-excitation energies were measured. Using PGOPHER simulations, the action scans placed the ν_3 fundamental mode at 914(7) cm^{-1}, yielding the first experimental measurement of this mode for TiO_2^-. From this experiment, we have demonstrated the success of applying this technique to TMOs with modes active in the far IR. We will follow up on this work by investigating larger TMO clusters, such as $Zr_2O_4^-$ and the water-split dissociative adducts $TiO_3H_2^-$ and $VO_3H_2^-$, further highlighting the importance of using gas-phase metal oxide clusters as model systems for catalytic reactions.

AUTHOR INFORMATION

Corresponding Author

†Daniel M. Neumark: dneumark@berkeley.edu

Authors Contributions

The manuscript was written through contributions of all authors. All authors have given approval to the final version of the manuscript.

Notes

The authors declare no competing financial interest.

Data Availability Statement.

The data that supports the findings of this study are available within the article and its supplementary material.

ACKNOWLEDGMENTS:

This research was funded by the Air Force Office of Scientific Research (AFOSR) under Grant no. FA9550-23-1-0545. Additional support was provided by CALSOLV, the center for solvation studies at the University of California, Berkeley. The authors would also like to acknowledge the Molecular Graphics and Computation Facility (MGCF) at Berkeley, funded by NIH S10OD034382, allowing us to run our QChem calculations. Q.-Y. Z. would also like to thank the College of Physical Science at Nankai University for providing support as an undergraduate visiting scholar at Berkeley. M. N. and M. H. acknowledge the support by the Deutsche Forschungsgemeinschaft (DFG, German Research Foundation) under the Research Training Group – GRK 2376–331085229 – "Confinement-Controlled Chemistry"

References:

1. G. Ertl, Angew. Chem. Int. Ed **47**, 3524–3535 (2008).
2. A. Khodakov, B. Olthof, A. T. Bell and E. Iglesia, J. Catal. **181**, 205–216 (1999).
3. I. Justicia, P. Ordejón, G. Canto, J. L. Mozos, J. Fraxedas, G. A. Battiston, R. Gerbasi and A. Figueras, Adv. Mater. **14**, 1399–1402 (2002).
4. A. Boffa, C. Lin, A. T. Bell and G. A. Somorjai, J. Catal. **149**, 149–158 (1994).
5. A. T. Bell and M. Head-Gordon, Annu. Rev. Chem. Biomol. Eng. **2**, 453–477 (2011).
6. A. W. Castleman, Catal. Lett. **141**, 1243–1253 (2011).
7. W. H. Robertson and M. A. Johnson, Annu. Rev. Phys. Chem. **54**, 173–213 (2003).

8. K. R. Asmis, Phys. Chem. Chem. Phys. **14**, 9270 (2012).
9. M. A. Duncan, Int. Rev. Phys. Chem. **22**, 407–435 (2003).
10. W. C. Lineberger, Annu. Rev. Phys. Chem. **64**, 21–36 (2013).
11. H. Wu and L. S. Wang, J. Chem. Phys. **107**, 8221–8228 (1997).
12. D. G. Leopold, K. K. Murray, A. E. S. Miller and W. C. Lineberger, J. Chem. Phys. **83**, 4849–4865 (1985).
13. D. M. Neumark, Phys. Chem. Chem. Phys. **7**, 433–442 (2005).
14. A. Osterwalder, M. J. Nee, J. Zhou and D. M. Neumark, J. Chem. Phys. **121**, 6317–6322 (2004).
15. D. M. Neumark, J. Phys. Chem. A **112**, 13287–13301 (2008).
16. M. L. Weichman and D. M. Neumark, Annu. Rev. Phys. Chem. **69**, 101–124 (2018).
17. H.-T. Liu, C.-G. Ning, D.-L. Huang, P. D. Dau and L.-S. Wang, Angew. Chem. Int. Ed. **52**, 8976–8979 (2013).
18. S. Yan, R. Zhang and C. Ning, J. Phys. Chem. Lett. **15**, 7735–7739 (2024).
19. J. B. Kim, M. L. Weichman and D. M. Neumark, Phys. Chem. Chem. Phys. **15**, 20973 (2013).
20. J. B. Kim, M. L. Weichman and D. M. Neumark, J. Chem. Phys. **140** (2014).
21. J. B. Kim, M. L. Weichman and D. M. Neumark, J. Am. Chem. Soc. **136**, 7159–7168 (2014).
22. M. C. Babin, M. DeWitt, J. A. Lau, M. L. Weichman, J. B. Kim, L. Cheng and D. M. Neumark, Phys. Chem. Chem. Phys. **24**, 17496–17503 (2022).
23. J. A. DeVine, A. Abou Taka, M. C. Babin, M. L. Weichman, H. P. Hratchian and D. M. Neumark, J. Chem. Phys. **148**, 222810 (2018).
24. A. Abou Taka, M. C. Babin, X. Sheng, J. A. DeVine, D. M. Neumark and H. P. Hratchian, J. Chem. Phys. **153**, 244308 (2020).
25. K. Vlahos, M. DeWitt and D. M. Neumark, Chin. J. Chem. Phys. **38**, 1–11 (2025).
26. K. Vlahos, M. DeWitt and D. M. Neumark, J. Phys. Chem. A **130**, 3037–3047 (2026).
27. D. M. Neumark, J. Phys. Chem. A **127**, 4207–4223 (2023).
28. M. DeWitt, M. C. Babin and D. M. Neumark, J. Phys. Chem. A **125**, 7260–7265 (2021).
29. J. A. Lau, M. DeWitt, M. A. Boyer, M. C. Babin, T. Solomis, M. Grellmann, K. R. Asmis, A. B. McCoy and D. M. Neumark, J. Phys. Chem. A **127**, 3133–3147 (2023).
30. M. DeWitt, D. Yang, J. A. Lau, K. Vlahos, H. Guo and D. M. Neumark, J. Phys. Chem. A **129**, 3682–3695 (2025).
31. J. A. Lau, M. DeWitt, P. R. Franke, J. F. Stanton and D. M. Neumark, J. Phys. Chem. A **129**, 1634–1647 (2025).
32. C. Hock, J. B. Kim, M. L. Weichman, T. I. Yacovitch and D. M. Neumark, J. Chem. Phys. **137**, 244201 (2012).
33. U. Even, J. Jortner, D. Noy, N. Lavie and C. Cossart-Magos, J. Chem. Phys. **112**, 8068–8071 (2000).
34. W. C. Wiley and I. H. McLaren, Rev. Sci. Instrum. **26**, 1150–1157 (1955).
35. A. T. J. B. Eppink and D. H. Parker, Rev. Sci. Instrum. **68**, 3477–3484 (1997).
36. D. W. Chandler and P. L. Houston, J. Chem. Phys. **87**, 1445–1447 (1987).
37. M. DeWitt, M. C. Babin, J. A. Lau, T. Solomis and D. M. Neumark, J. Phys. Chem. A **126**, 7962–7970 (2022).
38. B. Dick, Phys. Chem. Chem. Phys. **21**, 19499–19512 (2019).

39. C. Blondel, W. Chaibi, C. Delsart, C. Drag, F. Goldfarb and S. Kröger, Eur. Phys. J. D **33**, 335–342 (2005).
40. J. Cooper and R. N. Zare, J. Chem. Phys. **48**, 942–943 (1968).
41. K. L. Reid, Annu. Rev. Phys. Chem. **54**, 397–424 (2003).
42. A. Sanov, Annu. Rev. Phys. Chem. **65**, 341–363 (2014).
43. E. Epifanovsky, A. T. B. Gilbert, X. Feng, J. Lee, Y. Mao, N. Mardirossian, P. Pokhilko, A. F. White, M. P. Coons, A. L. Dempwolff, Z. Gan, D. Hait, P. R. Horn, L. D. Jacobson, I. Kaliman, J. Kussmann, A. W. Lange, K. U. Lao, D. S. Levine, J. Liu, S. C. McKenzie, A. F. Morrison, K. D. Nanda, F. Plasser, D. R. Rehn, M. L. Vidal, Z.-Q. You, Y. Zhu, B. Alam, B. J. Albrecht, A. Aldossary, E. Alguire, J. H. Andersen, V. Athavale, D. Barton, K. Begam, A. Behn, N. Bellonzi, Y. A. Bernard, E. J. Berquist, H. G. A. Burton, A. Carreras, K. Carter-Fenk, R. Chakraborty, A. D. Chien, K. D. Closser, V. Cofer-Shabica, S. Dasgupta, M. de Wergifosse, J. Deng, M. Diedenhofen, H. Do, S. Ehlert, P.-T. Fang, S. Fatehi, Q. Feng, T. Friedhoff, J. Gayvert, Q. Ge, G. Gidofalvi, M. Goldey, J. Gomes, C. E. González-Espinoza, S. Gulania, A. O. Gunina, M. W. D. Hanson-Heine, P. H. P. Harbach, A. Hauser, M. F. Herbst, M. Hernández Vera, M. Hodecker, Z. C. Holden, S. Houck, X. Huang, K. Hui, B. C. Huynh, M. Ivanov, Á. Jász, H. Ji, H. Jiang, B. Kaduk, S. Kähler, K. Khistyaev, J. Kim, G. Kis, P. Klunzinger, Z. Koczor-Benda, J. H. Koh, D. Kosenkov, L. Koulias, T. Kowalczyk, C. M. Krauter, K. Kue, A. Kunitsa, T. Kus, I. Ladjánszki, A. Landau, K. V. Lawler, D. Lefrancois, S. Lehtola, R. R. Li, Y.-P. Li, J. Liang, M. Liebenthal, H.-H. Lin, Y.-S. Lin, F. Liu, K.-Y. Liu, M. Loipersberger, A. Luenser, A. Manjanath, P. Manohar, E. Mansoor, S. F. Manzer, S.-P. Mao, A. V. Marenich, T. Markovich, S. Mason, S. A. Maurer, P. F. McLaughlin, M. F. S. J. Menger, J.-M. Mewes, S. A. Mewes, P. Morgante, J. W. Mullinax, K. J. Oosterbaan, G. Paran, A. C. Paul, S. K. Paul, F. Pavošević, Z. Pei, S. Prager, E. I. Proynov, Á. Rák, E. Ramos-Cordoba, B. Rana, A. E. Rask, A. Rettig, R. M. Richard, F. Rob, E. Rossomme, T. Scheele, M. Scheurer, M. Schneider, N. Sergueev, S. M. Sharada, W. Skomorowski, D. W. Small, C. J. Stein, Y.-C. Su, E. J. Sundstrom, Z. Tao, J. Thirman, G. J. Tornai, T. Tsuchimochi, N. M. Tubman, S. P. Veccham, O. Vydrov, J. Wenzel, J. Witte, A. Yamada, K. Yao, S. Yeganeh, S. R. Yost, A. Zech, I. Y. Zhang, X. Zhang, Y. Zhang, D. Zuev, A. Aspuru-Guzik, A. T. Bell, N. A. Besley, K. B. Bravaya, B. R. Brooks, D. Casanova, J.-D. Chai, S. Coriani, C. J. Cramer, G. Cserey, A. E. DePrince, III, R. A. DiStasio, Jr., A. Dreuw, B. D. Dunietz, T. R. Furlani, W. A. Goddard, III, S. Hammes-Schiffer, T. Head-Gordon, W. J. Hehre, C.-P. Hsu, T.-C. Jagau, Y. Jung, A. Klamt, J. Kong, D. S. Lambrecht, W. Liang, N. J. Mayhall, C. W. McCurdy, J. B. Neaton, C. Ochsenfeld, J. A. Parkhill, R. Peverati, V. A. Rassolov, Y. Shao, L. V. Slipchenko, T. Stauch, R. P. Steele, J. E. Subotnik, A. J. W. Thom, A. Tkatchenko, D. G. Truhlar, T. Van Voorhis, T. A. Wesolowski, K. B. Whaley, H. L. Woodcock, III, P. M. Zimmerman, S. Faraji, P. M. W. Gill, M. Head-Gordon, J. M. Herbert and A. I. Krylov, J. Chem. Phys. **155**, 084801 (2021).
44. S. Gozem and A. I. Krylov, Wiley Interdiscip. Rev. Comput. Mol. Sci. **12**, e1546 (2022).
45. C. M. Western, J. Quant. Spectrosc. Radiat. Transfer **186**, 221–242 (2017).